J Iber Geol (2017) 43:13–32
DOI 10.1007/s41513-017-0002-x

RESEARCH ARTICLE

Petrography, biomarker composition, mineralogy, inorganic geochemistry and paleodepositional environment of coals from La Ballesta mine, Peñarroya Basin, Spain

E. Lorenzo[1] · A. G. Borrego[2] · G. Márquez[3] · F. González[4] · C. Moreno[4]

Received: 10 March 2016 / Accepted: 3 February 2017 / Published online: 22 March 2017

Abstract
Purpose The purpose of this work is to study coal samples from various exposed seams of the La Ballesta mine, at the southeastern edge of the Peñarroya-Belmez-Espiel coalfield, southwestern Spain. Shaly seat- and caprocks were also investigated.
Method Petrographic, palynological, and biomarker analyses were carried out. The major elements were determined by X-ray fluorescence (XRF). The trace elements were analyzed by inductively coupled plasma-mass spectrometry (ICP-MS).
Results The Pennsylvanian (Westphalian)-age, high volatile bituminous coal studied is a humic coal with vitrinite concentrations of over 86% on a minerals-free basis and low amounts of liptinite and inertinite. The coals have a relatively higher volatile matter yields than the bituminous coals in western areas of the basin with similar vitrinite reflectance values and present both a dark and a light variety of vitrinite. The dark variety is more abundant in the low ash coals considered to have been formed in nearby lacustrine settings. The mineral assemblage of the coals and non-coal (roof and floor) rocks from the La Ballesta mine is dominated by quartz, kaolinite and illite, with minor to trace proportions of epigenetic carbonates, anatase, and K-feldspar, among others.
Conclusions Concentrations of B and B/Be ratios, along with other data, suggest that the La Ballesta coals may have originated from topogenous mires that developed next to lacustrine settings. Coal seams 9, 9bis, and 14 were probably more restricted systems than coaly shale 15, the latter corresponding to swamps associated with alluvial and floodplain environments. Abnormally high concentrations of trace elements such as Li, Rb, Cs, Sc, V and Cr might be explained by the input of detrital minerals into the Peñarroya Basin from the outcropping Precambrian and Lower Palaeozoic rocks to the northeast. In this regard, elemental ratios such as Al_2O_3/TiO_2 for the samples suggest that the modes of occurrence of the trace elements, and the minerals, in La Ballesta coals and non-coal rocks are to be mainly attributed to detrital input from felsic to intermediate metamorphic rocks.

Keywords Bituminous C coal · La Ballesta mine · Peñarroya–Belmez–Espiel coalfield · Petrography · Geochemistry

Resumen
Objetivo El objetivo de este trabajo es estudiar una serie de muestras de carbón de varios mantos aflorantes de la mina La Ballesta, en el margen suroriental de la cuenca minera de Peñarroya-Belmez-Espiel, suroeste de España. Las correspondientes lutitas infra- y suprayacentes también fueron investigadas.
Métodos Análisis petrográficos, palinológicos y de biomarcadores fueron realizados. Los elementos mayoritarios se analizaron por fluorescencia de rayos X (XRF). Los

✉ G. Márquez
gonzalo.marquez@diq.uhu.es

[1] Facultad de Ingeniería, Universidad Estatal Península de Santa Elena, Vía La Libertad-Santa Elena s/n, 7047 La Libertad, Ecuador

[2] Instituto Nacional del Carbón, INCAR-CSIC, C/Francisco Pintado Fe 26, 33011 Oviedo, Spain

[3] Departamento de Ingeniería Minera, Mecánica y Energética, Universidad de Huelva, La Rábida, 21819 Huelva, Spain

[4] Departamento de Geología, Universidad de Huelva, Campus de El Carmen, 21071 Huelva, Spain

elementos traza se analizaron por espectrometría de masas con plasma acoplado inductivamente (ICP-MS).
Resultados El carbón bituminoso alto volátil de edad Pensilvánica (Westfaliense), extraído en la zona de La Ballesta, es un carbón húmico con concentraciones de vitrinita de más del 86% en base libre de materia mineral y bajas cantidades de liptinita e inertinita. Estos carbones tienen una proporción de materia volátil relativamente mayor que en el caso de los carbones bituminosos de las parte occidental de la cuenca en estudio, pero poseen similares valores de reflectancia de la vitrinita, y presentan una variedad oscura y otra clara de vitrinita. La variedad oscura es más abundante en los carbones con bajo contenido en ceniza que se han formado en las cercanías de un medio lacustre. La mineralogía de carbones y lutitas (infra- y suprayacentes) de la mina La Ballesta está dominada por el cuarzo, caolinita e illita, con proporciones menores a trazas de carbonatos epigenéticos, anatasa y feldespato potásico, entre otros.
Conclusiones Las concentraciones de B y ratios B/Be, entre otros datos, sugieren que los carbones de La Ballesta se habrían formado a partir de cenagales que se desarrollaron junto a lagos. Los carbones 9, 9bis, and 14 se relacionan probablemente con sistemas más restringidos que en el caso de la lutita carbonosa 15; correspondiendo esta última con pantanos asociados con ambientes aluviales y llanuras de inundación. Unos valores anormalmente altos de las concentraciones de elementos traza tales como Li, Rb, Cs, Sc, V y Cr se pueden explicar por el aporte de minerales detríticos en la Cuenca Belmez-Espiel Peñarroya procedentes del afloramiento hacia el noreste de rocas de edad Precámbrica y Paleozoica temprana. A este respecto, relaciones elementales tales como Al_2O_3/TiO_2 sugieren que el origen de los elementos traza y las fases minerales, en carbones y lutitas de La Ballesta, pueden ser principalmente atribuido al aporte de detritos derivados de rocas metamórficas de tipo félsico a intermedio.

Palabras clave carbón bituminoso C · mina La Ballesta · cuenca Peñarroya-Belmez-Espiel · petrografía · geoquímica

1 Introduction

The Penarroya–Belmez–Espiel coalfield, also known as Peñarroya Basin (province of Córdoba, Andalusia, SW Spain) is a Moscovian strike-slip basin at the SE of the Iberian Variscan Massif. The convergence process that resulted in the Upper Palaeozoic Pangea formation produced transtensional forces in which strike-slip basins aligned with the main Variscan structures were formed (Stampfli and Borel 2002). These basins, of Pennsylvanian to Early Permian age, lay over different basements according to their respective location (Colmenero et al. 2002), and are all filled with continental deposits of alluvial, fluvial or/and lacustrine facies including some workable coal beds such as those in the Puertollano Basin (Jiménez et al. 1999) or in the Peñarroya–Belmez–Espiel Basin (Marques 2002; Suárez-Ruiz et al. 2006), the southeasternrmost part of which is the object of this study.

From the standpoint of coal mining industry, the Peñarroya–Belmez–Espiel coalfield has been divided into two different sectors: a western sector that has been known for its significant quantities of anthracite coal of late Langsettian (Westphalian A) to early Duckmantian (Westphalian B) age, and it is located northwestward from Peñarroya-Pueblonuevo (see Fig. 1), and an eastern sector on which deposits of middle Moscovian (late Duckmantian/Westphalian B after Wagner and Álvarez-Vázquez 2010) bituminous coal have been exploited (Wagner 2004). The La Ballesta mine is located in the southeastern edge of the basin, approximately 40 km southeast of the city of Peñarroya-Pueblonuevo (Fig. 1) and has remained unexplored until recently (1993) despite the fact that it contains the largest coal resources in the Peñarroya Basin (Álvarez-Vázquez 1995). The La Ballesta open-cast mine (Empresa Nacional Carbonífera del Sur, ENCASUR) extracted close to 0.5 Mt of coal per year from the early 1990s to 2010. The coal was burned in a 323 MW power plant, installed near the coal mine in the late 1960s.

Earlier investigations of the Peñarroya–Belmez–Espiel coals, summarized by Suárez-Ruiz and Jiménez (2004), focused mostly on samples from the Peñarroya-Pueblonuevo and Belmez–Espiel depositional areas, and included petrographic analyses (Marques 1993, 2002), and paleobotanical and palynological investigations (Álvarez-Vázquez 1995; Coquel 2004; Wagner and Álvarez-Vázquez 2010; among others), as well as chemical and mineralogical studies and an assessment of their utilization properties (Suárez-Ruiz et al. 2006). These studies have shown that the Peñarroya–Belmez–Espiel coals are often high in ash yield (up to 45%) and vitrinite-rich (60–90% vitrinite) and contain balanced amounts of liptinite and inertinite with liptinite normally dominating over inertinite (Marques 2002). The rank of the coals range between bituminous A and anthracite B (ISO 11760 2005) for the westernmost part of the basin, and is bituminous C for the area between Belmez and Espiel (Marques 1993, 2002). The main mineral phases identified in the Peñarroya bituminous coals are quartz and clay minerals (kaolinite and illite), minor traces of anatase and epigenetic carbonates, whereas the anthracites have significant amounts of epigenetic carbonates and kaolinite generated as a consequence of fluid circulation related to magmatic activity (Suárez-Ruiz et al. 2006). In contrast, studies of the La Ballesta coals are very scarce, i.e. only paleobotanical, organic geochemical and palynological studies have been carried out by Álvarez-Vázquez (1995), Lorenzo (2012), and González et al. (2016), respectively.

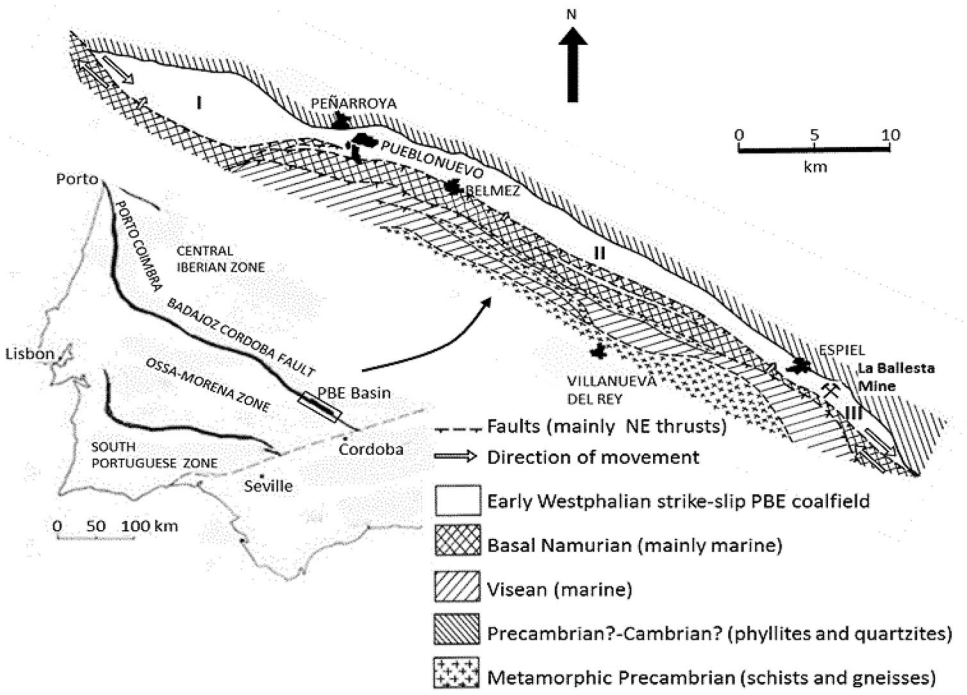

Fig. 1 Location of the Peñarroya Basin in SW Spain. *Outline map* showing the location of the La Ballesta mine and the relative position of successive basinal areas in the Peñarroya–Belmez–Espiel (PBE) coalfield. Successive basinal areas are labelled as I, II and III (modified from Wagner 2004)

Previous palynological data in the La Ballesta mine denote that these coals have originated from mires in strike-slip basins are tectonically controlled, but not by variations in the plant precursors. Therefore, a multidisciplinary study of the samples should be done. The aims of the present paper are, (1) to present a combination of organic petrographic, palynologic, and organic geochemical data from the La Ballesta samples in order to facilitate the interpretation of the depositional paleoenvironments and the peat-forming vegetation present during development of the studied La Ballesta seams; (2) to determine the mineralogical composition of both the coal seams and seat- and roof rocks, and (3) to measure and interpret the concentrations, origin and modes of occurrence of the major, minor and trace elements contained in the coals and related sediments.

2 Geological setting

The Peñarroya–Belmez–Espiel coalfield is a narrow strip of Pennsylvanian rocks (see Fig. 1), 1 km wide and 50 km long, parallel to the major Variscan structures of the Ossa–Morena zone in the Iberian Massif (Ortuño 1971). The Basin is located along the Badajoz-Córdoba fault zone (Martínez-Poyatos 2002), a region of intense tectonic deformation associated to numerous fault belts (Ortuño 1971). The northern boundary is marked by the outcrops of pre-Carbonifeorus basement composed of interbedded phyllites and quartzites and the southern boundary is a tectonic contact with marine detrital carbonates of Mississipian Age (Wagner 1999). The basin has a strongly asymmetrical profile with a wide normally dipping flank and a narrow steeply dipping opposed flank at the South-southwestern side, typical of a strike-slip basin (Wagner 2004), whose formation is associated to the late phases of the Hercynian orogeny. The shear movement of the thrust was responsible for changes in the depocentre of the basin south-eastwards leading to compartmentalization into three basinal areas (Wagner 2004; Wagner and Álvarez-Vázquez 2010). The basinal area I (close to Peñarroya-Pueblonuevo) is up to 0.5 Ma (Wagner 2004) older and was tectonically deformed before the development of basinal areas II (between Belmez and Espiel) and III (located southeast of Espiel and contains La Ballesta mine; Fig. 1).

The macrofloral composition of the Peñarroya–Belmez–Espiel Basin has been analyzed and documented in previous studies (e.g., Álvarez-Vázquez 1995). The basinal area I has been dated as late Langsettian-early Duckmantian (Álvarez-Vázquez 1995) on the basis of plant megafossils. It is noteworthy that the late Duckmantian floral composition of the La Ballesta area is almost identical to palaeoequatorial floras of the same age in the Paralic Coal Belt of northern Europe and North America (Wagner and Álvarez-Vázquez 2010). The biostratigraphically most significant genera reported in these studies were, among others, Corynepteris and Discopteris (ferns), Lepidodendron and Sigillaria (lycopsids), Calamites and Annularia (sphenopsids), Eusphenopteris and Cordaites (gymnosperms). From combining the stratigraphical range of all these macroflora species, the SE sector of the basin was assigned to the mid-Moscovian (late Duckmantian), possibly extending to the early Bolsovian (Wagner 2013). The coal petrographic analysis showed diabase sill intrusions folded together with the sediments

before the establishment of the second basinal area, producing locally natural coke (Marques 1993). The actual rank of the coals in this sub-basin is anthracite C. Basinal area II to the south-east is of late Duckmantian age (Álvarez-Vázquez 1995) and it has less tectonic deformation, which is essentially restricted to a steepening of the dip to near vertical in the southwestern flank and some minor faults in the northeastern flank (Wagner 2004) with coals reaching a lower bituminous level of coalification (Marques 1993). There is no age difference between basinal areas II and III but a different stratigraphic succession and a somewhat different fold structure (Wagner 2004).

The stratigraphic record of the upper Bashkirian-to-Moscovian (Langsettian to early Bolsovian) period in the Peñarroya–Belmez–Espiel Basin consists of alternating lutites, sandstones, conglomerates, breccias, and coal beds. The general distribution of sedimentary facies is similar in the three basinal areas: alluvial fan deposits that formed along the northeast basin margin pass laterally into fluvial sediments, which grade into floodplain and lacustrine sediments near the southwest margin of the basin (Wagner 1999). The Peñarroya–Belmez–Espiel coalfield was described as a typical limnic basin by Gabaldón and Quesada (1986) who defined a palaeogeographical model with four different sedimentary domains: (1) alluvial fans, (2) fluviatile, (3) fluvio-palustrine, and (4) fluvio-lacustrine in which coal beds could have been generated.

The coal seams in La Ballesta section are usually thin, although some reach up to 1–2 m in thickness, and no significant partings occur within the coals, except in seam 9. Coal beds in this mine are numbered 0–20 from bottom to top (see Fig. 2). The stratigraphic column of the Middle Moscovian (late Duckmantian/Westphalian B) sedimentary rocks comprises thin bands of bituminous coal interbedded with shales, sandstones, conglomerates and breccias. The seams studied were the 9, 9*bis*, 14, and 15 (coaly shale), which are 1–2 m thick. Seam 9 consists of two separate coal beds, each of which is up to 1 m thick; seams 14 and 15 are 2 and 1.5 m thick; the currently submerged and inaccessible seams 7 and 8 are slightly thicker. Most of the other seams are thin, non-workable beds with thicknesses of less than 1 m. The roof and floor shales (Álvarez-Vázquez 1995) of the four studied seams were also analyzed for mineral and trace element content.

3 Methods

Seams Nos. 9, 9*bis*, 14, and 15 were sampled from the La Ballesta open-cast mine at coordinates 38°09′45″ N, 4°58′16″W. Each seam is represented by one whole-seam channel sample in accordance with the ASTM D-4596 (2007) norm. Eight additional samples of the associated roof and floor were also sampled for mineralogical and

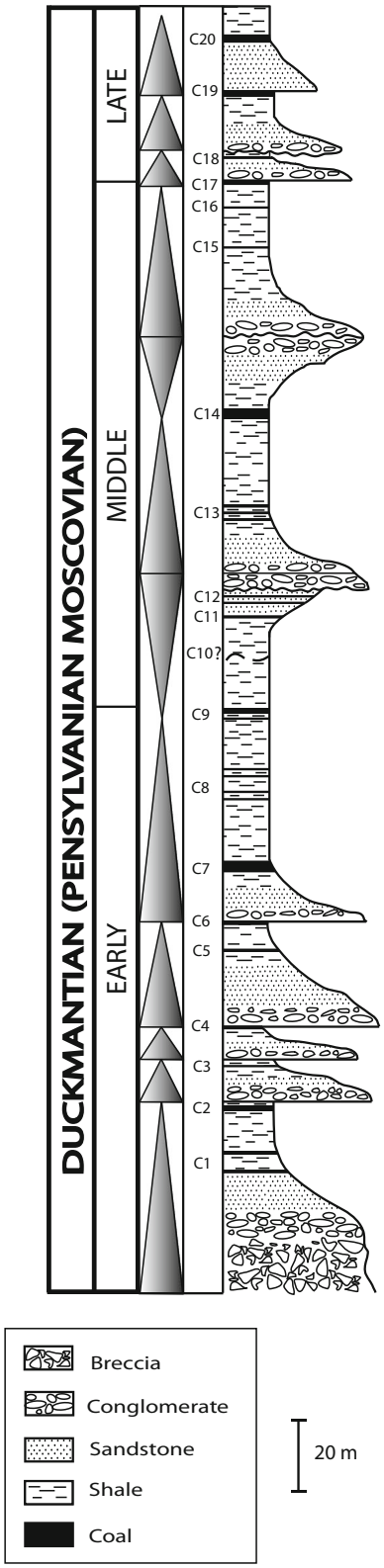

Fig. 2 Lithologic column for the La Ballesta mine showing the stratigraphic position of collected samples. Sequences have been indicated next to Duckmantian stages. The lowest coaly seam is symbolized by "C1", the next higher one is "C2", etc. (Álvarez-Vázquez 1995)

trace element analyses. The location of all the samples in the stratigraphic column is shown in Fig. 2. The samples (3 kg) were homogenised using a Jones jaw crusher to obtain a 100 g split of each sample.

Proximate analysis was completed using standards ISO 687 (2010) for moisture, ISO 562 (2010) for volatile matter, and ISO 1171 (2010) for ash yield; gross calorific value was determined using ISO 1928 (2009). The ultimate analysis was performed using ISO 29541 (2010) for C, H and N, ISO 19579 (2006) for total sulfur content, and a LECO Truspec micro O analyser for direct oxygen determination.

X-ray fluorescence (XRF) using Panalytical Axios equipment was used to determine S, Si, Al, Ca, Mg, K, Na, Fe, Mn and Ti on ashes obtained at 525 °C in an open muffle furnace (Hackley et al. 2005). Cl and Br were separately determined in the whole sample by X-ray fluorescence. In addition, trace elements (excluding mercury) were analysed by inductively coupled plasma mass spectrometry (ICP-MS) after the sample digestion process using an ultra clave microwave high pressure reactor (Milestone). The reagents for the 50-mg seam and roof/floor samples were 5-ml 65% HNO_3 and 2-ml 40% HF, as well as 2-ml 65% HNO_3 and 5-ml 40% HF, respectively. For boron analyses, samples were digested using HNO_3 mixed with H_3PO_4 and HF in order to reduce the volatilization of B after sample digestion. The memory effect of boron was eliminated by injecting a 2% ammonia solution into ICP-MS. Specifically, As and Se were determined in samples using collision/reaction cell technology (CCT) of ICP-MS following the method described by Li et al. (2014). Hg was determined by using a Milestone DMA-80 mercury analyzer. Multi-element standards (Inorganic Ventures CCS1, CCS4, CCS5, and CCS6; NIST 1633b and 2685b) were used to calibrate trace element concentrations.

Mineralogical analyses of the low-temperature ash coal samples were performed by X-ray diffraction (XRD) using a Bruker-AXS D8 Advance diffractometer equipped with a copper filament, CuKα radiation, tube conditions of 40 kV and 30 mA, $\Delta 2\theta = 3$–$70°$, step size = 0.03°, time step = 0.1 s, variable slit, 0.1 mm nickel filter and lynxeye linear detector. The diffractograms were obtained using the powder technique. The organic matter was removed from each seam sample by low-temperature oxygen-plasma ashing (LTA) following the USGS method (Kolker et al. 2003). The roof and floor samples were analysed by X-ray diffraction, without applying the plasma-ashing procedure. The clay minerals in the LTA residues from the Ballesta mine were analyzed separately. The LTA residues were dispersed in water treated with sodium hexametaphosphate and left settling in order to concentrate the fraction below 2 μm in effective diameter. Later, oriented-aggregate XRD was applied, after treatment with ethylene glycol and heating to 550 °C (Brown 1961), to investigate the composition of the clay fractions.

24-hour bitumen extraction was completed for each coaly sample in a Soxhlet apparatus using recently distilled (over calcium chloride) dichloromethane as solvent. After concentration of the extract using a rotary evaporator, it was separated into its constituent fractions (SARA method; Jewell et al. 1974). Asphaltenes were precipitated with *n*-heptane (in a 1:40 v/v ratio), saturates were eluted with *n*-hexane, aromatics with toluene, and resins using toluene/methanol (70:30 v/v). Aliquots of aliphatic and aromatic hydrocarbons were subsequently analysed by gas chromatography-mass spectrometry (GC–MS) using a 7890A GC System (Agilent Technologies) coupled to a 5975C Inert XL MSD equipped with a Triple-Axis Detector (Agilent Technologies). Gas chromatography was performed on capillary columns DB-1 ms (for saturates) and DB-5 ms (5% phenyl 95% dimethylpolysiloxane; for aromatic compounds), 60 m × 0.25 mm i.d. × 0.1 μm film, from Agilent Technologies. The initial oven temperature was 50 °C (held for 2 min) and then it was ramped at 2.5–300 °C where it was held for 70 min. The mass spectrometer was operated in electron ionization mode (EI) at 70 eV.

Optical microscopy was performed on particulate pellets (<1 mm grain size) following the ISO 7404-2 (2009) norm for sample preparation, ISO 7404-5 (2009) for vitrinite reflectance measurement and ISO 7404-3 (2009) for maceral analysis which was performed at a submaceral group level for vitrinite and at maceral level for inertinite and liptinite using the latest ICCP nomenclature (ICCP 1998, 2001). Random reflectance of vitrinite was measured for rank determination averaging 100 readings following the ISO 7404-5 (2009) standard.

4 Results and discussion

4.1 Depositional paleoenvironment and precursor organic matter

4.1.1 Coal utilization parameters

The seam samples show low moisture of analysis (1.6–2.0%), but very large differences in ash (3–74%) and volatile yields (43–52%), as shown in Table 1. The prefixes "S, F, and R" correspond to the seam, floor and roof samples. Three of them (9, 9bis and 14) can be considered coals according to ISO 11765 (2005) classification, with ash yields ranging from very low (seams 9 and 9 bis) to moderate (seam 14), whereas seam 15 should be classed as a carbonaceous shale. The volatile matter yield of the three coals is around 43% dry-ash-free (daf), which places the

Table 1 Proximate and ultimate analyses and gross calorific values (MJ kg^{-1} on a moist-ash-free basis) of La Ballesta seam samples

Sample	Moisture (wt%)	Ash yield (db%)	Volatile matter (daf%)	Fixed carbon	C (db%)	H (db%)	N (db%)	O (db%)	St (db%)	Calorific value	H/C[a]	O/C[a]	C/N
S9	1.8	3.4	43.0	55.0	79.85	5.59	1.62	8.08	0.58	34.66	0.84	0.09	49.29
S9*bis*	1.8	3.9	43.6	54.2	79.21	5.40	1.65	9.14	0.60	34.98	0.83	0.08	48.01
S14	2.0	19.7	42.5	46.2	70.18	4.82	1.58	8.04	0.53	37.17	0.82	0.08	44.42
S15	1.6	74.1	56.9	11.2	15.54	1.86	0.39	5.24	0.14	26.19	1.47	0.25	39.85

wt% weight percentage, *db* dry basis, *daf* dry-ash-free basis

[a] Atomic ratio

coals at the boundary between high volatile bituminous C and B according to the Teichmüller's (1987) equivalence of rank parameters. The gross calorific values are significantly higher for the coals than those established for the high volatile bituminous rank interval in the ASTM D-388 (2011) system (24.4–32.6 MJ kg^{-1} on a moist-ash-free basis), indicating certain anomalies in the characterization parameters of the coals. The significantly higher volatile matter yield of seam 15 is attributed to errors incurred when calculating the results on a dry, ash-free basis for a sample that is primarily ash (74%). The H/C atomic ratios indicate coals with relatively high hydrogen content. All the coals have a low total sulfur content (St <1 wt%), which is typical of coals from limnic depositional environments (Barnerjee and Goodarzi 1990). The studied coals have a higher volatile matter yield than the bituminous coals from basinal area II (Suárez-Ruiz et al. 2006), which may be explained by the fact that the carbonates can contribute to volatile matter determination. The ash yields of those coals were intermediate between those of Seam 9 and Seam 15.

As can be seen in Fig. 3, when the H/C and O/C atomic values are plotted on the Van Krevelen diagram, the coals plot over the track corresponding to Type III kerogen. Compared with coals of the western areas of the basin (Suárez-Ruiz et al. 2006), the La Ballesta coals have lower O/C ratios (partially attributable to the lower oxygen contents resulting from direct measurement) and slightly higher H/C ratios compared to those of coals with a lower volatile matter yield (34–40% daf; Suárez-Ruiz et al. 2006) indicating the H-enrichment of these coals. The high C/N ratios for all the coals (Table 1) are typical of humic coals (Meyers and Ishiwatari 1993).

4.1.2 *Preservation of organic components*

The macroscopic appearance of the coal corresponds mainly to vitrain with some areas showing alternating bright and dull bands of clarain. The carbonaceous shale has a grey appearance, is well-laminated and heavy, with occasional organic partings. Reflectance was measured on

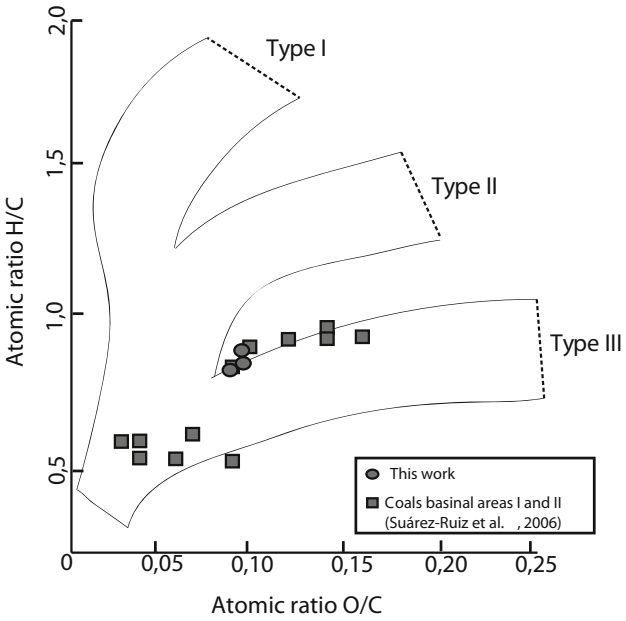

Fig. 3 Van Krevelen diagram (Tissot and Welte 1984) showing data for the three coal samples

collotelinite. During the course of the analysis it became clear that there were two kinds of vitrinite, a dark and a light variety, which are present not only in the collotelinite but also other vitrinite macerals. The existence of a dark and light variety of vitrinite in coals is common in particular at low ranks, but the differences tend to be minimized as rank increases. The reflectance histograms indicate a relatively large dispersion of values from 0.54 to 0.90% (Fig. 4), which is rather large for coals in this rank interval, but they also show the Modes for the dark and light vitrinite populations (Fig. 4).

As shown in Fig. 5b, c the light and dark varieties appear close together within the grains and are not associated to weathering cleats or fissures or alteration rims that might lend support to a reflectance difference caused by a recent weathering process. Palaeo-desiccation of woody components at the time of deposition under conditions, which were not as severe as those required for the formation of inertinite (Taylor et al. 1989), might be an

explanation for this difference in reflectance. Nevertheless these processes are often associated to environments with contrasted seasons, generally resulting in coals with relatively high inertinite content as observed in Permian Gondwana coals (Diessel 2010). In addition slitted structures typical of the so-called pseudovitrinite (Benedict et al. 1968; O'Keefe et al. 2013) do not characterize the light vitrinite in these coals.

Alternatively the light vitrinite could be considered as rank vitrinite, which is usually the case in relatively lower rank coals and the dark variety would either result from a strongly reducing H-rich environment, such perhydrous vitrinite (Stach et al. 1982; Iglesias et al. 2000) or from a different plant type. One of the options for the hydrogen-enrichment of vitrinite is coexistence with high contents of liptinite, whose bituminous substances can migrate into the vitrinite, resulting in a lower reflectance (Kalkreuth 1982). In the present case, this option has to be ruled out given the low liptinite content of the samples (Table 2). Perhydrous vitrinites have also been identified in sapropelic reducing environments, commonly associated with high tissue destruction levels (Diessel and Gammidge 1998) and in less acidic environments, related to marine transgressions

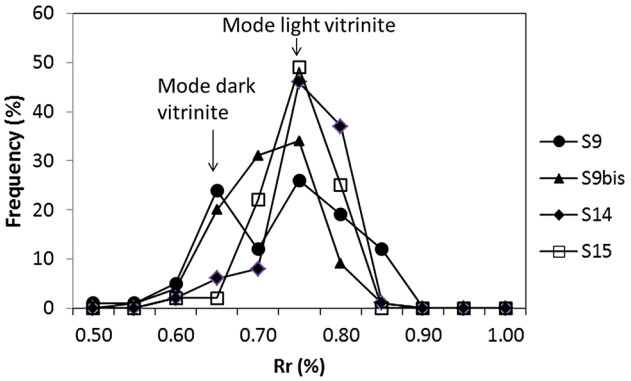

Fig. 4 Histograms of vitrinite reflectance indicating the Modes corresponding to the reflectance of the dark and light vitrinite

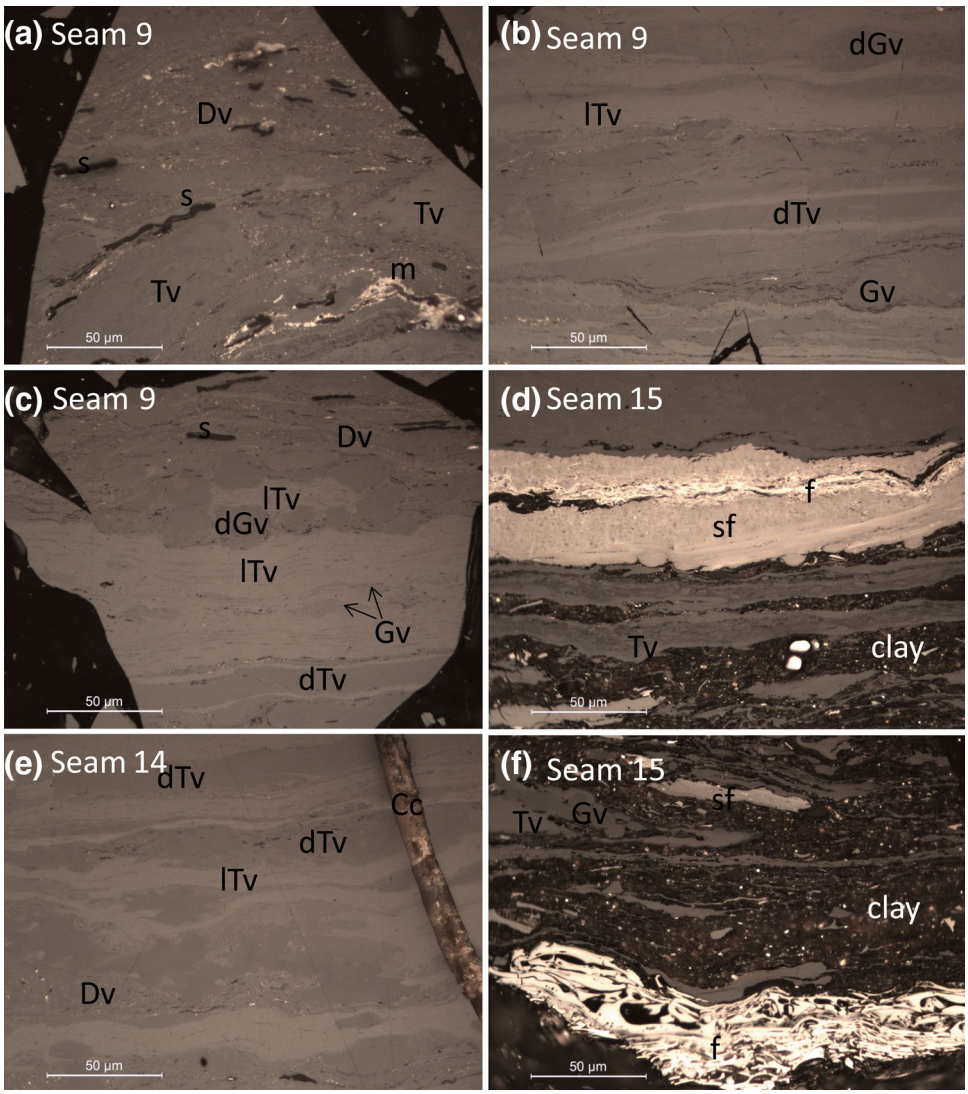

Fig. 5 Reflected light oil immersion images of the maceral occurrences in the studied samples. *Dv* detrovitrinite, *Tv* telovitrinite, *Gv* gelovitrinite, *sf* semifusinite, *f* fusinite, *s* sporinite, *cc* carbonates. Prefix "d" and "l" refers to dark and light component, respectively

as observed in the Permian coals from the Gunnedah basin (Gurba and Ward 1998). The low sulfur contents and high level of tissue preservation (high telovitrinite) does not support this hypothesis in this study. Moreover, because of its association with tissues and resinous fillings, the vitrinite may also become darker (Suárez-Ruiz et al. 1994). This phenomenon has been described mainly for Mesozoic and post-mesozoic coals associated with the widespread occurrence of resinous-rich conifers (Gentzis and Goodarzi 1994). A different chemistry in the wood precursor of the vitrinites could also be responsible for the darker appearance and the reflectance retardation observed (Petersen and Rosenberg 1998). Lycopsid periderm (bark) in Carboniferous coals is one of the main contributors to vitrinite (DiMichele and Philips 1994) and is a very resistant tissue often impregnated by resinous substances (DiMichele and Philips 1988). This vitrinite can be expected to be darker than that derived from cordaiteans, calamiteans or medullosans plants. Detailed studies on etched surfaces of coals (Winston 1986), which have revealed the internal structure of telovitrinite bands, have shown that corpogelinite cell-fillings of lycopods may be either lighter or darker than the cell-walls and that corpogelinite in ferns is commonly darker than the cell-walls (Winston 1988). This would affect the reflectance of lycopod-, cordaitean- or fern-derived telovitrinite bands, although there has been no systematic study on this topic to the author's knowledge. The high tissue preservation index (>2) observed in the samples and the low inertinite content would be typical of waterlogged environments with possibly low pH and low oxidation levels within forested peatlands or forested wet raised bogs (Diessel 1992). Indeed the relative proportion of light vitrinite increases with the increase in mineral matter indicating that those seams that had more detrital input were those that had a higher amount of lighter vitrinites. The different density of plants generating dark vitrinite or the different chemistry of plants in waterlogged environments could explain the distribution of reflectances found in the seam samples.

Compared with the coals from basinal area II within the basin, the maceral composition of La Ballesta seams is similar to that of coal seam 5 in the proximity of Belmez (Marques 2002), but La Ballesta seams are generally richer in vitrinite, have remarkably lower inertinite contents and generally a lower liptinite content (Marques 2002) than most of the bituminous coals in basinal area II and they have one of the highest tissue preservation levels. The rank of the coals would be that of the light vitrinite population (ca. 0.78%) for all the samples measured because there is no shift observed in the modal values of the light population among the samples.

Table 2 Petrographic results of the seam samples. Maceral terminology according to ICCP (1998, 2001)

Maceral/component	S9	S9*bis*	S14	S15
Telovitrinite (vol.% mfb)	68.7	71.3	62.9	43.9
Detrovitrinite (vol.% mfb)	18.2	22.4	21.6	40.5
Gelovitrinite (vol.% mfb)	11.6	5.0	1.7	4.1
Fusinite (vol.% mfb)	0.0	0.0	0.1	1.3
Semifusinite (vol.% mfb)	0.1	0.3	4.0	4.4
Micrinite (vol.% mfb)	0.1	0.1	0.4	0.4
Sporinite (vol.% mfb)	1.3	0.9	9.3	8.1
Total vitrinite (vol.% mfb)	98.5	98.7	86.2	85.8
Dark vitrinite (vol.% mfb)	53.2	47.4	3.3	0.0
Light vitrinite(vol.% mfb)	45.3	51.3	82.9	85.8
Total inertinite (vol.% mfb)	0.2	0.4	4.5	6.1
Total liptinite (vol.% mfb)	1.3	0.9	9.3	8.1
Light vitrinite/total vitrinite	0.46	0.52	0.96	1.00
Rr (%)	0.73	0.76	0.78	0.77

%Rr equals to vitrinite reflectance

mfb minerals-free basis, *vol.* volume

4.1.3 *Biomarker assemblage*

The bitumen yields obtained range from 1.5 to 3.5% of the extracted coaly rock samples, averaging 2.5%, of which 8–10% were aliphatic hydrocarbons, 11–13% were aromatics, and 77–80% were asphaltenes plus resins. No strong variations within the chromatograms of the different samples were found. Combined gas chromatographic-mass spectrometric analyses of the saturates showed a similar *n*-alkane distribution in all extracts (Fig. 6); i.e., a unimodal distribution pattern from *n*-C_{15} to *n*-C_{31} without odd/even predominance, with the maximum peaks between *n*-C_{18} and *n*-C_{21}, which typical of mature coals (Fleck et al. 2001). Also bacterial *n*-alkane, supported by the presence of hopanes (Peters et al. 2005), could be contributing to the medium chain length *n*-alkanes.

Pristane is the most abundant hydrocarbon compound in all the samples, and the pristane to phytane ratio ranges from 3.0 to 4.1 (Table 3), which is typical of humic coals (Tissot and Welte 1984).

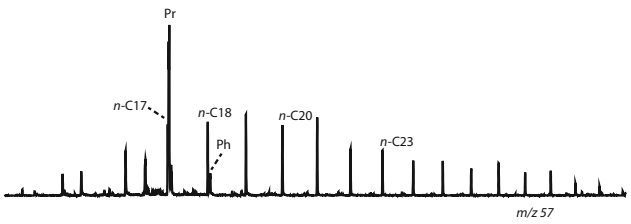

Fig. 6 Example (S14 sample) of m/z 57 mass fragmentogram of the saturated fraction of the La Ballesta coaly rock extracts

In this context, Pr/Ph values over 3 and dibenzotiophene to phenanthrene—DBT/P—ratios lower than unity (see Table 3; Fig. 7a) are compatible with peat deposition in topogenous mires within fluvio-lacustrine settings (Hughes et al. 1995; O'Keefe et al. 2013). The high abundance of 1,2,5,6-(and co-eluting 1,3,6,7-) tetramethylnaphthalene isomers and 1,2,5-trimethylnaphthalene (Fig. 7b, peak identifications shown in Table 4) have been attributed to microbial (Borrego et al. 1997; Jiang et al. 1998) and/or higher plant inputs (van Aarssen and de Leeuw 1992). Also, the presence of bacterial-derived hopanoids (Ourisson and Albrecht 1992) and the notable quantity of drimane-type bicyclic sesquiterpanes (Fig. 8a) seems to reflect significant contributions by bacterial organic matter (Noble 1986). Regarding triterpanes, the studied coal seams show a dominance of hopanes with 17α21β configuration and low amounts of moretanes ranging from C_{29} to C_{31} (Fig. 8b, peak identifications are given in Table 4).

4.1.4 *Paleoecology and depositional setting*

In palaeocogical terms, the palynological assemblages and the palaeobotanical data previously reported (Álvarez-Vázquez 1995; González et al. 2016) provide a good qualitative and quantitative representation of the major Carboniferous floristic groups: lycopsids, sphenopsids, ferns, and gymnosperms (Table 5). Nevertheless, the palynological grouping results of seams 9, 14 and 15 reveal strong variations in the quantitative distribution of the palynofloras (González et al. 2016).

Table 3 Molecular parameters for the saturates and aromatics in sampled coaly rocks from the La Ballesta mine

	S9	S9*bis*	S14	S15
Pr/Ph	3.1	3.0	3.6	4.1
Pr/*n*-C_{17}	3.6	3.5	3.2	3.4
Ph/*n*-C_{18}	0.4	0.4	0.4	0.4
%22*S*	61	60	59	59
DBT/P	0.05	0.07	0.15	0.10
MPI-1	0.65	0.66	0,64	0,62
Reflectance (%Rc_1)	0.79	0.79	0.78	0.77
DNR	3.33	3.31	3.28	3.27
Reflectance (%Rc_2)	0.79	0.78	0.77	0.77
Beyerane/homodrimane	0.12	0.13	0.16	0.19
Hopane/moretane	1.5	1.5	1.3	1.4
MNR	1.2	1.2	1.1	1.0

% 22S or C_{31} regular homohopane 22S/(22S + 22R) ratio; MPI-1 = 1.5·(2-MP + 3-MP)/(P + 1-MP + 9-MP); assuming Rc_1 in the range 0.65–1.35% (Radke et al. 1982a), MNR = 2-MN/1-MN; %Rc_1 = 0.4 + 0.6·MPI-1; DNR = (2,6-DMN + 2,7-DMN)/1,5-DMN; and %Rc_2 = 0.49 + 0.09·DNR

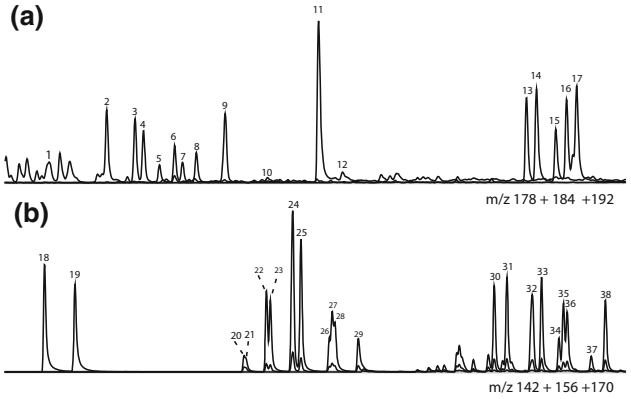

Fig. 7 **a**, **b** m/z 178 + 184 + 192 and m/z 142 + 156 + 170 mass fragmentograms for the aromatic fraction the S14 sample

La Ballesta seams can be grouped following the palynologic-petrographic-geochemical method reported in Eble et al. (1994). Although other authors (e.g., Moore and Shearer 2003) have reported that these types of indicators are not always applicable, we consider this method to be valid in this case because the coals in this study are roughly coeval with those examined by Eble et al. (1994). Coal seam 9 is largely dominated by lycopsid spores (>90% of the assemblage) and vitrinite (98%; Table 2) and can be classified in the lycopsid-vitrinite dominant group (high vitrinite, over 80% of lycopsid spores with ash yields below 10%). Coal seam 14 falls into the mixed palynoflora-vitrinite dominant group with a high vitrinite and low ash yield, but a more diverse palynomorph assemblage (10% lycopsids and 60% sphenopsids), suggesting the presence of topogenous mires. Finally, coaly shale seam 15 falls into the mixed palynoflora-high ash yield group with palynoflora co-dominated by lycopsids (28%), sphenopsids (34%) and ferns (36%), suggesting an intermittently dry, probably stressed environment with a much higher input of detrital material into a topogenous mire system, perhaps an open swamp associated with alluvial and floodplain environments. It must be pointed out, however, that on a whole-count basis, no increase in inertinite content is observed in seam 15, although it is apparent when the data are examined on a minerals-free basis. Seams 14 and 15 are also those with negligible amounts of dark vitrinite. These latter results, coupled with a minor qualitative variation in the plant precursors (Álvarez-Vázquez 1995), suggest that maceral distribution can also be explained by changes in environmental pH/Eh conditions (Rimmer and Davis 1988; O'Keefe et al. 2013).

The La Ballesta area was located close to the equator during the mid-Moscovian (late Duckmantian) times (Golonka et al. 1995). An intertropical climate with variable humidity was present, as indicated by the presence of hygrophytic (Calamites, Lepidodendrales and Sigillarias)

Table 4 Main aromatic compounds, triterpanes, bicyclic sesquiterpanes and tetracyclic diterpanes identified in the fragmentograms

1 1,3,5,7-Tetramethylnaphthalene	31 1,3,6-Trimethylnaphthalene
2 1,3,6,7-Tetramethylnaphthalene	32 1,3,5-Trimethylnaphthalene*
3 1,2,4,6-Tetramethylnaphthalene	33 2,3,6-Trimethylnaphthalene
4 1,2,5,7-Tetramethylnaphthalene	34 1,2,7-Trimethylnaphthalene
5 2,3,6,7-Tetramethylnaphthalene	35 1,6,7-Trimethylnaphthalene
6 1,2,6,7-Tetramethylnaphthalene	36 1,2,6-Trimethylnaphthalene
7 1,2,3,7-Tetramethylnaphthalene	37 1,2,4-Trimethylnaphthalene
8 1,2,3,6-Tetramethylnaphthalene	38 1,2,5-Trimethylnaphthalene
9 1,2,5,6-Tetramethylnaphthalene*	39 8β(H)-Drimane
10 Dibenzothiophene	40 8β(H)-Homodrimane
11 Phenanthrene	41 17-Nortetracyclane
12 Anthracene	42 *ent*-Beyerane
13 3-Methylphenanthrene	43 16β(H)-Phyllocladane
14 2-Methylphenanthrene	44 Abietane
15 2-Methylanthracene	45 *ent*-Kaurane
16 9-Methylphenanthrene	46 16α(H)-Phyllocladane
17 1-Methylphenanthrene	47 17α(H)-22,29,30-Trisnorhopane
18 2-Methylnaphthalene	48 17α(H),21β(H)-30-Norhopane
19 1-Methylnaphthalene	49 17β(H),21α(H)-30-Normoretane
20 2-Ethylnaphthalene	50 17α(H),21β(H)-Hopane
21 1-Ethylnaphthalene	51 17β(H),21α(H)-Moretane
22 2,6-Dimethylnaphthalene	52 17α(H),21β(H)-29-Homohopane 22S
23 2,7-Dimethylnaphthalene	53 17α(H),21β(H)-29-Homohopane 22R
24 1,3-Dimethylnaphthalene*	54 17β(H),21α(H)-29-Homomoretane 22S + 22R
25 1,6-Dimethylnaphthalene	55 17α(H),21β(H)-29-Bishomohopane 22S
26 1,4-Dimethylnaphthalene	56 17α(H),21β(H)-29-Bishomohopane 22R
27 2,3-Dimethylnaphthalene	57 17α(H),21β(H)-29-Trishomohopane 22S
28 1,5-Dimethylnaphthalene	58 17α(H),21β(H)-29-Trishomohopane 22R
29 1,2-Dimethylnaphthalene	59 17α(H),21β(H)-29-Tetrahomohopane 22S
30 1,3,7-Trimethylnaphthalene	60 17α(H),21β(H)-29-Tetrahomohopane 22R

Peak co-elution in asterisks

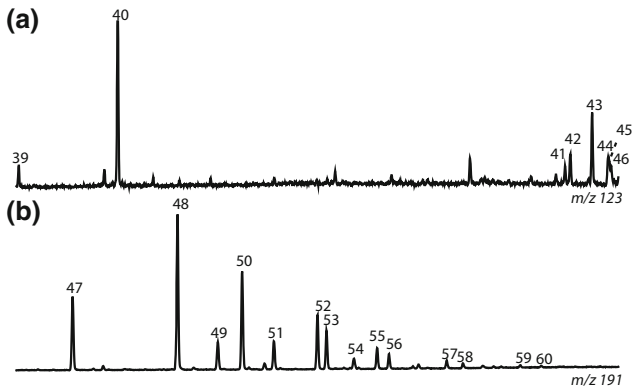

Fig. 8 **a**, **b** m/z 123 and m/z 191 mass fragmentograms showing drimanes and sesquiterpanes, as well as triterpanes for the representative S9 sample

and mesophytic flora (Cordaitales; Izart et al. 2012). Cordaites are known to occur in both mire and upland settings (DiMichele et al. 2008). An input of extrabasinal elements (*Rhacopteris bipinnata* and *Rhodeites gutbieri*, among others) has been reported from the Peñarroya–Belmez–Espiel Basin (Wagner and Álvarez-Vázquez 2010). The occurrence of these upland elements is likely related to the fact that the Peñarroya–Belmez–Espiel coalfield is a local, fairly narrow intramontane basin, with evidence of upstanding basin margins with alluvial fans (Andreis and Wagner 1983).

The two phyllocladane isomers are biomarkers typical of Serpukhovian and younger ages (Fabianska et al. 2003). The dominance of 16β(H)-phyllocladane and *ent*-beyerane over the other related tetracyclic diterpanes (Fig. 7a) could imply a limited contribution by Cordaitales, and possibly Voltziales, to the parent organic matter of the studied samples. However, no remains of volztialean conifers have been found in the La Ballesta coals. Although poor specific biomarkers such as cadalene, retene and *ent*-kauranes can derive from numerous Carbonifeorus higher plants (Peters et al. 2005), phyllocladanes, *ent*-beyerane and

Table 5 Palynologic and palaeobotanical taxa reported in La Ballesta assigned to the four major floristic groups. Data compiled from Álvarez-Vázquez (1995) and González et al. (2016)

	Palynology	Paleobotany
Lycopsids	*Cirratriradites saturni*	*cf. Eleutherophyllum waldenburgense*
	Densosporites annulatus	*Lepidodendron aculeatum*
	D. Spheaerotriangulatus	*L. mannebachense*
	Endosporites ornatus	*Ulodendron acutum*
	E. zonalis	*Bothrodendron minutifolium*
	Crassispora konsankei	*Lepidophloios laricinus*
	Lycospora pusila	*Sigillaria boblayi*
		S. daureuxii
		S. ovata
		Asolanus camptotaenia
		Flemingites russelianus
		Lepidostrobus ornatus
		Lepidostrobophyllum lanceolatum
		Sigillariostrobus rhombibracteatus
Sphenopsids	*Calamospora microrugosa*	*Calamites carinatus*
	C. mutabilis	*C. cistii*
	Laevigatosporites minor	*C. suckowii*
	L. vulgaris	*Annularia jongmansii*
	Vestispora tortuosa	*A. ramosa*
		Asterophyllites charaeformis
		A. grandis
		A. longifolius
		Calamostachys charaeformis
		C. germanica
		Palaeostachya elongata
		Macrostachya hauchecornei
		Sphenophyllum cuneifolium
		S. kidstonii
		S. wingfieldense
		Bowmanites cuneifolius
Ferns	*Apiculastiporis abditus*	*Corynepteris coralloides*
	Dyctiotriletes densoreticulatus	*C. essinghii*
	D. medioreticulatus	*C. similis*
	Granulatisporites granulatus	*Urnatopteris herbacea*
	G. microgranifer	*Renaultia crepinii*
	Leiotriletes priddyi	*R. footneri*
	Lophotriletes gibbosus	*R. schatzlarensis*
	Raistrickia fulva	*Zeilleria avoldensis*
	R. superba	*Z. frenzlii*
	R. saetosa	*Z. hymenophylloides*
	Reticulatisporites carnosus	*Discopteris karwinensis*
	R. polygonalis	*D. opulenta*
	R. reticulatus	*D. vuellersii*
	Savatrisporites nux	*Senftenbergia plumosa*
	Verrucosisporites cerosus	*Pecopteris volkmansii*
	V. sifati	
	Cyclogranisporites multigranus	

Table 5 continued

	Palynology	Paleobotany
Gymnosperms	*Florinites junior*	*Neuropteris guadiatensis*
	F. mediapudens	*Laveineopteris aff. Tenuifolia*
	F. pumicosus	*Paripteris gigantea*
	Monoletes ellipsoides	*Lonochopteris rugosa*
		Alethopteris valida
		Mariopteris muricata
		Karinopteris obtusifolia
		Eusphanopteris obtusiloba
		E. sauveurii
		E. scribani
		Palmatopteris furcata
		P. schatzlarense
		Sphenopteris artemissiaefolia Cordaites principalis
		Dorycordaites palmaeformis

2-methylretene are more specific biomarkers, as they are related to conifers and probably arborescent lycopsids (Romero-Sarmiento et al. 2011). Last, the seam samples showed neither eudasmane nor arborane- nor fernane-derivates, which have been detected in Asturian (Westphalian D) or younger coals (Vliex et al. 1994) and have been related to the occurrence of cordaites, pteridosperms, and early conifers (Auras et al. 2006).

4.2 Depositional setting and provenance of inorganic components

Figure 9 shows the X-ray diffractograms of the LTA seam residues. The mineralogy of the seams is quite uniform. The main minerals present are quartz and clays (kaolinite and illite). These three primary minerals are probably detrital in nature (Ward and Christie 1994; Dai et al. 2013a) as observed in Fig. 5d, f where they are interbedded with the macerals, although they have also been described as derived from authigenic processes (Ward 1989; Vassilev et al. 1994). The dominant clay mineral is kaolinite with subordinate illite, which is even less abundant in seam 14 (see oriented aggregate XRD traces of LTA clay fractions in Fig. 10). Minor minerals identified in the coal samples include anatase, K-feldspar, and iron-bearing carbonates (ankerite and siderite). These carbonates are the dominant iron-bearing compounds in coals that are very low in pyrite (Ward et al. 2001) in accordance with the freshwater depositional environment in which the coals were formed (Kemezys and Taylor 1964). Carbonates can be considered

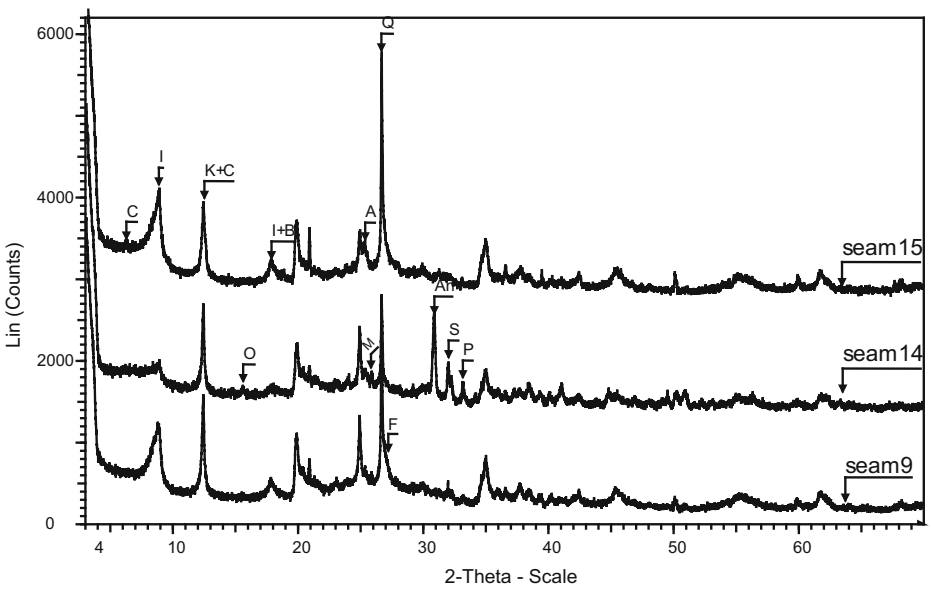

Fig. 9 X-ray powder diffractograms of LTA obtained from selected coaly samples. *Q* quartz; *K* kaolinite; *S* siderite; *I* illite; *F* feldspar; *C* chlorite; *D* dolomite; *H* hematite; *A* Anatase; *M* mereiterite; *O* orschadite; *P* pyrite; and *B* butlerite

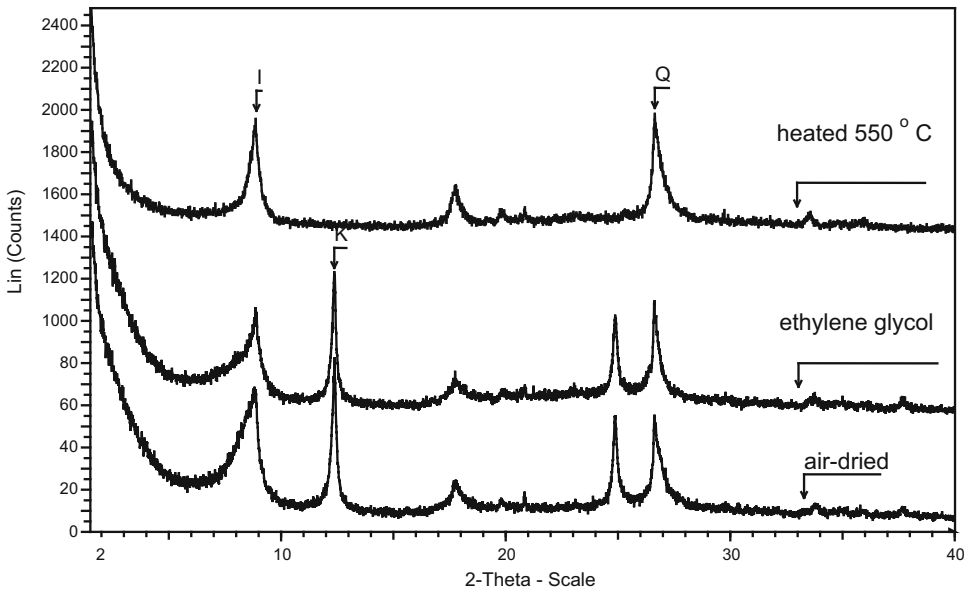

Fig. 10 Oriented-aggregate X-ray diffractograms of the clay fraction of the LTA from a representative La Ballesta coal, showing d-spacing of peaks in Ångstroms: *Bottom* air-dried; *centre* saturated with ethylene glycol; *top* heated to 550 °C

authigenic minerals that precipitated during the early diagenesis (Ward et al. 1996). This is supported by their ocurrence in cleats or cavities as shown in Fig. 5e. They are absent in coaly shale seam 15. Ankerite is associated with siderite as calcium availability decreases in the water solutions at a late stage in the coaĺs history (Ward et al. 2001). Traces of muscovite and pyrite were also noted in the LTA residues of seams 9 and 14 whereas chlorite, pyrite and anatase were found in seam 15. Muscovite is commonly unstable during coal formation and may have transformed to clay minerals (Vassilev et al. 1994). Furthermore, traces of hematite and several sulfates (mereiterite, orschadite and butlerite) that probably formed during the LTA process (Alastuey et al. 2001) were detected. The under- and over-lying shales show no important vertical variations in mineralogy and also consist mostly of quartz, kaolinite, and illite, with minor minerals such as siderite and calcite.

Table 6 shows the concentrations of major and minor element oxides on a dry, ash basis for the La Ballesta seams, floor and roof rocks. Table 7 presents the results of the multielemental analyses performed for the bituminous coals and shales under study, as well as Swaine's worldwide ranges of trace elements identified in the three coal samples, the S15 coaly shale and non-coal rocks. We quantified 30 trace elements, in particular 14 (Sb, Be, As, Se, Cr, Cl, Cd, Co, Pb, Mn, Ni, Th, Hg, and U; excluding F) out of the 15 potentially hazardous trace elements (PHTEs) identified by the United States Environmental Protection Agency in 1990.

The Al_2O_3-to-TiO_2 ratio is used as provenance indicator of sedimentary rocks (Hayashi et al. 1997) and of the sediment-source region for coal deposits (Dai et al. 2015b). The Al_2O_3-to-TiO_2 ratios between 17 and 48 for the La Ballesta coals and the roof and floor rocks indicate that their sediment-source region was mainly of felsic and, in some cases, intermediate composition. La/Cr and Th/Sc ratios that do not exceed one also suggest that the modes of occurrence of the trace elements, and the minerals, in the non-coal rocks may be due to detrital input from felsic to intermediate metamorphic rocks (Piovano et al. 1999).

Concentrations of the PHTEs in all the coal samples are generally found within the worldwide concentration ranges of trace elements in coal (see Tables 6, 7), except for the slightly high Co, Hg and Cr contents. Therefore, considering the PHTEs concentrations in La Ballesta coals, these 14 elements might pose significant potential risks for the human health and environment. Also, in accordance with literature (Suárez-Ruiz et al. 2006), we observed abnormally high Nd, Sm, Cu, Li, Rb, Cs, Sc, V, Co, and Cr concentrations outside the range of values for these elements found in most coals of the world. Taking into account the major mineral phases present in La Ballesta coals and the association of the majority of these elements with clay minerals (Stanton and Finkelman 1995), the respective anomalous concentrations can be explained by the input of detrital minerals into the Peñarroya–Belmez–Espiel Basin from the outcropping Precambrian and Lower Palaeozoic rocks to the northeast (Suárez-Ruiz et al. 2006). When the concentrations of trace elements for the studied coals are compared with those of their respective Clarke values reported by Ketris and Yudovich in 2009 (see Table 8), nearly all trace elements analyzed fall between 1/6x and 6x, and they cannot therefore be considered depleted or enriched according to the criterion proposed by Gluskoter et al. (1977). Only two elements show values between 6 and 8 times greater than the Clarke values in La Ballesta coals (Table 8). The PHTEs concentrations

Table 6 Composition in weight % (except Cl and Br in μg/g) of all the ash samples

Sample	HTA	SiO_2	Al_2O_3	Fe_2O_3	MnO	MgO	CaO	Na_2O	K_2O	TiO_2	SO_3	Cl[a]	Br
S9	5.31	40.75	29.83	6.26	0.08	6.41	10.10	0.57	3.27	0.66	1.12	462.7	82.3
S9*bis*	5.42	40.56	29.91	6.34	0.08	6.43	10.05	0.55	3.29	0.62	1.21	465.8	84.0
S14	28.67	51.93	28.80	7.02	0.10	1.77	4.90	0.32	2.49	1.04	0.96	126.6	21.1
S15	76.82	58.73	28.03	2.98	0.01	1.36	2.49	0.47	4.41	1.08	0.03	32.2	2.2
F9	–	68.82	20.51	3.75	0.07	1.24	0.73	0.24	3.35	1.04	0.07	10.1	0.1
R9	–	69.40	16.80	5.70	0.05	1.70	1.97	0.26	2.80	0.89	0.11	13.3	0.1
F9*bis*	–	68.58	20.72	3.49	0.08	1.26	0.78	0.25	3.33	1.07	0.06	11.8	0.2
R9*bis*	–	69.77	16.99	5.32	0.05	1.65	2.02	0.27	2.70	0.94	0.10	12.4	0.1
F14	–	68.75	20.91	3.81	0.04	1.12	0.45	0.32	3.28	1.04	0.04	18.5	0.1
R14	–	68.97	20.66	3.10	0.03	1.21	0.36	0.32	3.43	1.06	0.07	12.9	0.1
F15	–	73.17	16.68	4.36	0.07	0.93	0.30	0.16	2.87	0.96	0.10	17.2	0.1
R15	–	64.95	22.94	3.96	0.03	1.44	0.35	0.32	4.18	1.00	0.08	23.0	0.2

[a] The world average Cl contents (ash basis) in hard coal and shale are 1435 and 150 μg/g (Yudovich and Ketris 2006)

(except Cd, Pb, Hg and U) in the S15 coaly shale are higher than in the La Ballesta coals.

The coal samples show concentrations of B from 40 to 53 μg/g and B/Be ratios around 17, suggesting that the La Ballesta coals were formed in peat swamps developed in fresh to negligibly brackish water habitats (Goodarzi and Swaine 1994), which is coherent with the low total sulfur content, significant levels of fluvial trace elements (Ba, Ce, Cu, Cr, Fe, K, La, Mn, Nd, Ni, Sr, Sm, Th, V, and Zr; Wedepohl 1978), and the inferred topogenous mire depositional environment of the parent organic matter. However, the concentration of B in coal may be derived from hydrothermal fluids (Lyons et al. 1989), volcanic activity (Karayigit et al. 2000) and acid waters (Dai et al. 2015a), or it may be due to climatic variations (Bouška and Pešek 1983). Despite these drawbacks, the boron content has been used as paleosalinity indicator, although it must be interpreted with caution. Boron can show a mixed organic and inorganic (mainly illite) affiliation (Dai et al. 2014). Regarding most likely modes of occurrence of other trace elements in La Ballesta coals, Cr and V are presumably occur in association with organic matter, and to a lesser extent, associated with illite (Liu et al. 2015). Ba, Cs, Li and Rb may be present in clay minerals (Shao et al. 2003), while Be concentrations close to Clarke values may be associated with clay minerals detected in the LTA residues (Dai et al. 2015c). The Na in these coals might be related to the organic matter (Ward et al. 1999) or pore solutions (Spears and Zheng 1999). The concentration of U is probably controlled by the organic matter in La Ballesta coals (Shao et al. 2003), though this element may be hosted in a series of uranium minerals (Dai et al. 2015d). The enrichment of Hg in the studied coals would indicate that the influence of hydrothermal processes on the geochemistry of La Ballesta seams cannot be fully ruled out (Dai et al. 2013b). In regards to the shaly seat- and caprocks, elemental concentration is rather uniform with depth and the floors are similar in composition to the roofs. Also, the studied non-coal rocks of the La Ballesta mine are slightly depleted in the majority of the trace elements relative to the Clarke values for shales (Table 8). In addition, ashes of La Ballesta coals have lower concentrations of some trace elements (V, Ni, As and Cr; among others) when compared to the shales associated with the coal seams. This might be explained by the presence of different mineral phases in non-coal rocks.

4.3 Thermal maturity indices

Vitrinite reflectance is considered the best rank parameter since it is measured on individually identified components, it is not affected by maceral composition of the coal, it is not reverted with complex geological histories (Stach et al. 1982) and vitrinite is ubiquitously present. Indeed in the samples studied vitrinite is the major maceral group with low proportions inertinite and low to moderate proportions of liptinite (Table 2). As previously shown vitrinite in these coals was heterogeneous with both a light and a dark population. The dark population predominated in the coals generated in a more lacustrine or marginally lacustrine environment (seams 9 and 9*bis*), whereas the light population predominated in the seams associated with alluvial and flood plain environments (coal seam 14 and coaly shale 15). If the light population is considered as the rank population, the Mode is in the interval 0.75–0.79%, whose mid-value would be 0.77% (Fig. 4). In accordance with Borrego et al. (2000), the volatile matter yield of vitrinites with a reflectance of 0.77% would be 38%, which is lower than that measured in the proximate analyses. The estimated volatiles of a vitrinite with a reflectance value of

Table 7 Trace element (μg/g) concentration in all the samples

	S9	S9*bis*	S14	S15	F9	R9	F9*bis*	R9*bis*	F14	R14	F15	R15	World coals[a]	Hard coals[b]	Shales[b]
Li	47.67	48.82	**82.57**[c]	83.14	37.58	40.48	43.09	39.75	36.19	43.49	29.17	46.29	1–80	14 ± 1	66
B	53.66	52.43	40.12	69.65	38.39	42.25	38.07	40.54	38.85	43.25	48.25	36.69	5–400	47 ± 3	100
V	**106.30**	**104.98**	**107.49**	114.18	100.30	84.42	108.61	94.26	89.00	110.96	96.87	120.51	2–100	28 ± 1	130
Cr	**65.88**	**65.06**	**68.45**	69.72	95.47	80.75	111.74	99.90	96.57	107.75	91.14	118.74	0.5–60	17 ± 1	90
Co	**34.08**	**33.81**	**30.17**	11.46	11.23	23.19	14.34	15.92	23.16	17.05	16.57	27.47	0.5–30	6.0 ± 0.2	19
Ni	44.42	43.79	45.46	54.28	44.89	76.50	53.88	60.97	66.28	70.16	48.86	82.98	0.5–50	17 ± 1	68
Cu	**53.25**	**53.00**	**56.41**	46.92	30.88	15.31	21.55	33.04	24.85	39.77	26.49	39.55	0.5–50	16 ± 1	45
Zn	98.63	96.94	106.45	58.28	155.10	113.49	133.22	139.15	127.83	169.03	131.25	154.61	5–300	28 ± 2	95
As	3.73	3.95	4.30	4.37	5.49	4.42	5.16	4.73	4.38	10.85	4.84	6.99	0.5–80	9.0 ± 0.7	13
Rb	**111.06**	**109.67**	**114.85**	134.57	158.47	169.24	141.79	156.03	144.88	119.07	148.96	173.73	2–50	18 ± 1	140
Sr	150.93	152.24	170.71	195.43	158.45	135.85	145.46	152.94	150.71	209.04	157.09	132.78	10–500	100 ± 7	300
Zr	21.53	21.02	31.15	46.42	111.01	130.74	123.12	135.43	153.26	192.28	170.59	144.57	5–200	36 ± 3	160
Mo	2.72	2.56	1.91	2.29	1.11	1.90	1.79	2.00	0.98	1.12	1.27	1.48	0.1–10	2.1 ± 0.1	2.6
Cs	1.30	1.21	**5.33**	4.97	3.07	2.98	3.72	2.99	3.22	2.08	3.08	3.71	0.3–5	1.10 ± 0.12	5
Sc	3.92	4.10	**19.28**	27.52	11.12	7.92	10.90	8.16	9.95	8.78	10.27	9.17	1–10	3.7 ± 0.2	13
Sb	2.14	2.01	2.35	3.10	0.45	0.42	0.48	0.43	0.55	0.57	0.47	0.76	0.1–10	1.00 ± 0.09	1.5
Ba	279.62	290.33	463.35	249.42	406.92	452.38	418.21	446.64	495.16	505.64	504.02	488.58	20–1000	150 ± 10	580
La	31.86	30.18	33.33	40.83	38.23	28.33	40.05	30.14	33.18	71.03	43.53	51.92	1–40	11 ± 1	92
Ce	64.77	62.93	69.12	45.99	83.22	60.47	81.89	61.73	72.21	100.56	97.93	106.93	2–70	23 ± 1	59
Nd	**34.80**	**34.10**	**37.27**	24.16	31.48	33.48	31.90	33.03	29.27	27.81	38.08	30.27	3–30	12 ± 1	16
Sm	**7.80**	**7.85**	**8.45**	9.28	5.61	4.48	5.19	4.81	5.46	4.77	5.61	5.50	0.5–6	2.2 ± 0.1	6.4
Pb	27.45	26.96	28.34	17.90	31.18	29.39	29.80	27.45	16.36	22.98	23.28	21.05	2–80	9.0 ± 0.7	20
U	1.25	1.23	1.10	1.44	0.69	0.42	0.73	0.55	0.82	0.90	0.89	0.51	0.5–10	1.9 ± 0.1	0.9
Be	3.38	3.15	3.63	4.47	2.55	2.18	2.49	2.20	2.48	2.22	1.94	2.25	0.1–15	2.0 ± 0.1	3
Th	1.56	1.69	5.30	17.89	20.6	18.5	20.1	17.9	20.2	19.6	18.4	17.8	0.5–10	3.2 ± 0.1	12
Ge	6.9	7.0	5.5	2.7	2.0	1.9	1.2	1.6	1.7	1.4	1.7	2.1	0.5–50	2.4 ± 0.2	1.6
Cd	0.33	0.37	0.22	0.28	0.19	0.21	0.08	0.18	0.23	0.16	0.20	0.14	0.2–10	0.20 ± 0.04	0.3
Hf	0.03	0.04	0.16	0.89	3.31	4.43	3.61	4.70	3.59	4.40	3.25	3.37	0.02–1.00	0.10 ± 0.01	2.8
Se	0.6	0.6	1.0	0.8	1.1	0.9	0.8	1.2	0.9	0.7	1.3	0.6	0.2–1.6	1.6 ± 0.1	0.5
Hg	0.60	0.62	0.72	0.39	0.04	0.07	0.09	0.05	0.08	0.03	0.06	0.03	0.02–1.00	0.10 ± 0.01	0.58

[a] Worldwide ranges in coal (Swaine 1990)

[b] Clarke values for bituminous coals and shales (Ketris and Yudovich, 2009)

[c] Values in boldface are higher than Swainés worldwide ranges

Table 8 Average enrichment pattern of trace elements in sampled coals and associated shales

K	Coals	Non-coal rocks
>6	Rb, Hg	–
>1	Li, B, V, Cr, Co, Ni, Cu, Zn, Sr, Cs, Sc, Cd, Sb, Ba, La, Ce, Nd, Sm, Pb, Be, Ge	Cr, Se, Zn, Rb, Ce, Th, Hf, Nd, Pb, Co, Ge
<1	U, Zr, Se, As, Hf, Mo, Th	Cu, Mo, Li, Sm, U, V, Be, Cs, Sb, B, Cd, Sr, Sc, Ba, Ni, As, La, Zr
<6	–	Hg

K: ratio of the element content to the Clarke value

0.67% (dark vitrinite) would be 42%, which is closer to the value obtained by the proximate analysis. When the La Ballesta coals are compared with those of basinal area II in the same basin where the volatile matter yields are 34–41% daf for coals with a vitrinite reflectance ranging from 0.66 to 0.90%, the perhydrous character of La Ballesta coals seems to be more evident. The biomarkers also provide maturity ratios that can be used to confirm the reflectance values. The hopane isomerization ratios for all extracts (%22*S*, Table 3) are around 0.6 indicating that the coals have only reached the early oil window. The predominance of 8β(H)-epimers of homodrimane and drimane (Fig. 8a) in all samples is in agreement with vitrinite reflectance values higher than 0.7% (Noble et al. 1987). The methylphenanthrene indices (MPI-1; Radke et al. 1982a), as well as both the dimethylnaphthalene ratios (DNR; Radke et al. 1994) and the methylnaphthalene ratios (MNR; Radke et al. 1982b), allow to estimate an equivalent vitrinite reflectance value of ~0.78% (see Table 3), which agrees with the measured values for the light vitrinite population.

5 Conclusions

The results of the petrologic, mineralogical, elemental and organic geochemical study on the sampled seams in La Ballesta mine lead to the following conclusions:

1. Petrographic and biomarker data suggest that the coal facies correspond to topogenous mire environments, which vary from more restricted paleomires systems (coal seams 9 and 9*bis*) to swamps mainly associated with marginal lacustrine settings (coal seam 14), or swamps associated with alluvial and floodplain environments (coaly shale seam 15). These coals are among the vitrinite-richer and inertinite-poorer of those reported in the Peñarroya–Belmez–Espiel Basin. The coal-forming environments indicated by petrographic and geochemical results coincide with those deduced from the palynoflora.
2. La Ballesta coals have a moderate degree of maturity (Rr of about 0.77%), which is within the range of those reported in the basinal area II (between Belmez and Espiel) but they have comparatively higher volatile matter yield. The presence of vitrinite of different reflectances is attributed to distinctive composition of the plants, given the lack of specific desiccation/oxidation features that could account for these differences. The seams formed in more restricted areas with less detrital influence are those that have a higher proportion of dark vitrinite. The different density of plants generating dark vitrinite or the different chemistry of plants in waterlogged environments could explain the distribution of reflectances found in the seam samples. This vitrinite could be associated to lycopods, whose bark-like material forms vitrinite in Carboniferous coals and is highly resistant, which may be contributing to the high tissue preservation index observed in these coals.
3. The coal seams from the La Ballesta mine contain distinctive proportions of mineral matter, consisting of abundant quartz, kaolinite and illite, with minor proportions of anatase, feldspar and carbonate minerals. The similar mineralogy of the coal seams and the associated shales denotes that the mineral matter in the coals is mainly of detrital origin. Coaly, seat- and caprocks are enriched in some elements (Rb, Cr, Ni, and V) typical of clay minerals, which may be due to the input of detrital minerals into the Peñarroya–Belmez–Espiel coalfield from the outcropping Precambrian and Lower Palaeozoic rocks to the northeast. Finally, the various elemental ratios obtained for the La Ballesta coals and the shales suggest that their sediment-source region was mainly of felsic composition.

Acknowledgements Authors are grateful to the company ENCASUR for providing access to the samples. We are also grateful to the two anonymous reviewers for their comments which helped us to improve the original version of the manuscript.

References

Alastuey, A., Jiménez, A., Plana, F., Querol, X., & Suárez-Ruiz, I. (2001). Geochemistry, mineralogy and technological properties of the main Stephanian (Carboniferous) coal seams from the Puertollano Basin, Spain. *International Journal of Coal Geology, 45,* 181–195.

Álvarez-Vázquez, C. (1995). *The early Westphalian macroflora of the Peñarroya–Belmez–Espiel basin (Cordoba).* Unpublished Doctoral thesis. Oviedo (Spain): Universidad de Oviedo.

Andreis, R. R., & Wagner, R. H. (1983). Study of alluvial fans at the northern edge of the Westphalian B Peñarroya–Belmez basin (Córdoba). In M. J. Lemos de Sousa (Ed.), *Contributions to the carboniferous geology and paleontology of the Iberian Peninsula* (pp. 171–227). Oporto: Universidade do Porto.

ASTM International ASTM D 388 (2011). Standard classification of coals by rank. In *Annual book of ASTM Standards: petroleum products, lubricants, and fossil fuels; gaseous fuels; coal and coke*, *sec. 5, v. 5.06* (pp. 372–378). West Conshohocken: ASTM.

ASTM International ASTM D 4596 (2007). Standard practice for collection 01 channel samples of coal in a mine. In *Annual book of ASTM Standards: petroleum products, lubricants, and fossil fuels; gaseous fuels; coal and coke*, *sec. 5, v. 5.06*. West Conshohocken: ASTM.

Auras, S., Wilde, V., Hoernes, S., Scheffler, K., & Püttmann, W. (2006). Biomarker composition of higher plant macrofossils from Late Palaeozoic sediments. *Palaeogeography, Palaeoclimatology, Palaeoecology, 240,* 305–317.

Barnerjee, I., & Goodarzi, F. (1990). Paleoenvironment and sulfur–boron contents of the Mannville (Lower Cretaceous) coals of southern Alberta, Canada. *Sedimentary Geology, 67,* 297–310.

Benedict, L. G., Thompson, R. R., Shigo, J. J., & Aikman, R. P. (1968). Pseudovitrinite in Appalachian coking coals. *Fuel, 47,* 125–143.

Borrego, A. G., Blanco, C. G., & Püttmann, W. (1997). Geochemical significance of the aromatic distribution in the bitumens of the Puertollano oil shales. *Organic Geochemistry, 26,* 219–228.

Borrego, A. G., Marbán, G., Alonso, M. J. G., Álvarez, D., & Menéndez, R. (2000). Maceral effects in the determination of proximate volatiles in coals. *Energy and Fuels, 14,* 117–126.

Bouška, V., & Pešek, J., (1983). Boron in the aleuropelites of the Bohemian massif. In *5th meeting of the European clay groups (Prague)* (pp. 147–155).

Brown, G. (1961). *The X-ray identification and crystal structures of clay minerals*. London: Mineralogical Society.

Colmenero, J. R., Fernández, L. P., Moreno, C., Bahamonde, J. R., Barba, P., Heredia, N., et al. (2002). Carboniferous. In W. Gibbons & T. Moreno (Eds.), *Geology of Spain* (pp. 120–153). London: The Geological Society of London.

Coquel, R. (2004). Etude palynologique du Westphalien du basin houiller de Peñarroya–Bélmez–Espiel, Espagne (Andalousie). *Palaeontographica Abteilung, B, 267,* 1–18.

Dai, S., Liu, J., Ward, C. R., Hower, J. C., Xie, P., Jiang, Y., et al. (2015a). Petrological, geochemical, and mineralogical compositions of the low-Ge coals from the Shengli Coalfield, China: A comparative study with Ge-rich coals and a formation model for coal-hosted Ge ore deposit. *Ore Geology Reviews, 71,* 318–349.

Dai, S., Seredin, V. V., Ward, C. R., Hower, J. C., Xing, Y., Zhang, W., et al. (2015b). Enrichment of U–Se–Mo–Re–V in coals preserved within marine carbonate successions: geochemical and mineralogical data from the Late Permian Guiding Coalfield, Guizhou, China. *Mineralium Deposita, 50,* 159–186.

Dai, S., Song, W., Zhao, L., Li, X., Hower, J. C., Ward, C. R., et al. (2014). Determination of boron in coal using closed-vessel microwave digestion and inductively coupled plasma mass spectrometry (ICPMS). *Energy and Fuels, 28,* 4517–4522.

Dai, S., Wang, P., Ward, C. R., Tang, Y., Song, W., Jiang, J., et al. (2015c). Elemental and mineralogical anomalies in the coal-hosted Ge ore deposit of Lincang, Yunnan, southwestern China: Key role of N_2–CO_2-mixed hydrothermal solutions. *International Journal of Coal Geology, 152,* 19–46.

Dai, S., Yang, J., Ward, C. R., Hower, J. C., Liu, H., Garrison, T. M., et al. (2015d). Geochemical and mineralogical evidence for a coal-hosted uranium deposit in the Yili Basin, Xinjiang, northwestern China. *Ore Geology Reviews, 70,* 1–30.

Dai, S., Zhang, W. G., Seredin, V. V., Ward, C. R., Hower, J. C., Song, W. J., et al. (2013a). Factors controlling geochemical and mineralogical compositions of coals preserved within marine carbonate successions: A case study from the Heshan Coalfield, southern China. *International Journal of Coal Geology, 109,* 77–100.

Dai, S., Zhang, W., Ward, C. R., Seredin, V. V., Hower, J. C., Li, X., et al. (2013b). Mineralogical and geochemical anomalies of late Permian coals from the Fusui Coalfield, Guangxi Province, southern China: Influences of terrigenous materials andhydrothermal fluids. *International Journal of Coal Geology, 105,* 60–84.

Diessel, C. F. K. (1992). *Coal-bearing depositional systems*. Berlin: Springer.

Diessel, C. F. K. (2010). The stratigraphic distribution of inertinite. *International Journal of Coal Geology, 81,* 251–268.

Diessel, C. F. K., & Gammidge, L. (1998). Isometamorphic variations in reflectance and fluorescence of vitrinite—a key to depositional environment. *International Journal of Coal Geology, 36,* 167–222.

DiMichele, W. A., Kerp, H., Tabor, N. J., & Looy, C. V. (2008). The so-called "Paleophytic-Mesophytic" transition in equatorial Pangea-multiple biomes and vegetational tracking of climate change through geological time. *Palaeogeography, Palaeoclimatology, Palaeoecology, 268,* 152–163.

DiMichele, W. A., & Philips, T. L. (1988). Paleoecology of the Middle Pennsylvanian age Herrin coal swamp near a contemporaneous river system, the Walshville Paleochannel. *Review of Palaeobotany and Palynology, 56,* 151–176.

DiMichele, W. A., & Philips, T. L. (1994). Paleobotanical and paleoecological constraints on models of peat formation in the Late Carboniferous of Euramerica. *Palaeogeography, Palaeoclimatology, Palaeoecology, 106,* 39–90.

Eble, C. F., Hower, J. C., & Andrews, W. M., Jr. (1994). Paleoecology of the Fire Clay coal bed in a portion of the Eastern Kentucky coalfield. *Palaeogeography, Palaeoclimatology, Palaeoecology, 106,* 287–305.

Fabianska, M. J., Bzowska, G., Matuszewska, A., Racka, M., & Skret, U. (2003). Gas chromatography and mass spectrometry in goechemical investigation of organic matter of the Grodziec Beds (Upper Carboniferous), Upper Silesian Coal Basin (Poland). *Chemie der Erde-Geochemistry, 63,* 63–91.

Fleck, S., Michels, R., Izart, A., Elie, M., & Landais, P. (2001). Paleoenvironmental assessment of Westphalian fluvio-lacustrine deposits of Lorraine (France) using a combination of organic geochemistry and sedimentology. *International Journal of Coal Geology, 48,* 65–88.

Gabaldón, V., & Quesada, C. (1986). Examples de bassins houillers limniques du sud-ouest de la péninsule Ibérique: évolution sédimentaire et contrôle structural. *Mémoire de la Société géologique de France, 149,* 27–36.

Gentzis, T., & Goodarzi, F. (1994). Reflectance suppression in some Cretaceous coals from Alberta, Canada. In P. K. Mukhopadhyay & W. G. Dow (Eds.), *Vitrinite reflectance as a maturity parameter: Applications and limitations, ACS Symposium Series 570* (pp. 93–110).

Gluskoter, J. J., Ruth, R. R., Miller, W. G., Cahill, R. A., Dreher, G. B., & Kuhn, J. K. (1977). Trace elements in coal: occurrence and distribution. *III State Geological Survey Circular, 499,* 1–154.

Golonka, J., Ross, M. I., & Scotese, C. R. (1995). Phanerozoic paleogeographic and paleoclimatic modelling maps. *Canadian Society of Petroleum Geologists Memoir, 17,* 1–47.

González, F., Moreno, C., Lorenzo, E., & Márquez, G. (2016). Vegetation distribution and coal-forming environments in a strike-slip basin. The Pennsylvanian Peñarroya–Belmez–Espiel Basin, southern Spain. *Terra Nova, 28,* 171–180.

Goodarzi, F., & Swaine, D. J. (1994). Paleoenvironmental and environmental implications of the boron content of coals. *Geological Survey Canadian Bulletin, 471,* 1–76.

Gurba, L. W., & Ward, C. R. (1998). Vitrinite reflectance anomalies in high-volatile bituminous coals of the Gunnedah Basin, New South Wales, Australia. *International Journal of Coal Geology, 36,* 111–140.

Hackley, P. C., Warwick, P. D., & González, E. (2005). Petrology, mineralogy and geochemistry of mined coals, western Venezuela. *International Journal of Coal Geology, 63,* 68–97.

Hayashi, K. I., Fujisawa, H., Holland, H. D., & Ohmoto, H. (1997). Geochemistry of ~1.9 Ga sedimentary rocks from northeastern Labrador, Canada. *Geochimica et Cosmochimica Acta, 61,* 4115–4137.

Hughes, W. B., Holba, A. G., & Dzou, L. I. P. (1995). The ratios of dibenzothiophene to phenanthrene and pristane to phytane as indicators of depositional environment and lithology of petroleum source rocks. *Geochimica et Cosmochimica Acta, 59,* 3581–3598.

Iglesias, M. J., Jiménez, A., del Río, J. C., & Suárez-Ruiz, I. (2000). Molecular characterisation of vitrinite in relation to natural hydrogen enrichment and depositional environment. *Organic Geochemistry, 31,* 1285–1299.

International Committee for Coal and Organic Petrology (ICCP). (1998). The new vitrinite classification (ICCP System 1994). *Fuel, 77,* 349–358.

International Committee for Coal and Organic Petrology (ICCP). (2001). The new inertinite classification (ICCP System 1994). *Fuel, 80,* 459–471.

ISO 1171. (2010). *Solid mineral fuels—determination of ash*. Geneva: International Organization for Standardization.

ISO 11760. (2005). *Classification of coals*. Geneva: International Organization for Standardization.

ISO 1928. (2009). *Solid mineral fuels—determination of gross calorific value by the bomb calorimetric method and calculation of net calorific value*. Geneva: International Organization for Standardization.

ISO 19579. (2006). *Solid mineral fuels—determination of sulfur by IR spectrometry*. Geneva: International Organization for Standardization.

ISO 29541. (2010). *Solid mineral fuels—Determination of total carbon, hydrogen and nitrogen content—Instrumental method*. Geneva: International Organization for Standardization.

ISO 562. (2010). *Hard coal and coke—determination of volatile matter*. Geneva: International Organization for Standardization.

ISO 687. (2010). *Solid mineral fuels—coke—determination of moisture in the general analysis test sample*. Geneva: International Organization for Standardization.

ISO 7404-2. (2009). *Methods for the petrographic analysis of coals—part 2: Methods of preparing coal samples*. Geneva: International Organization for Standardization.

ISO 7404-3. (2009). *Methods for the petrographic analysis of coals—part 3: Method of determining maceral group composition*. Geneva: International Organization for Standardization.

ISO 7404-5. (2009). *Methods for the petrographic analysis of coals—part 5: Method of determining microscopically the reflectance of vitrinite*. Geneva: International Organization for Standardization.

Izart, A., Palhol, F., Gleixner, G., Elie, M., Blaise, T., Suárez-Ruíz, I., et al. (2012). Palaeoclimate reconstruction from biomarker geochemistry and stable isotopes of *n*-alkanes from Carboniferous and Early Permian humic coals and limnic sediments in western and eastern Europe. *Organic Geochemistry, 43,* 125–149.

Jewell, D. M., Albaugh, E. W., Davis, B. E., & Ruberto, R. G. (1974). Integration of chromatographic and spectroscopic techniques for the characterization of residual oils. *Industrial and Engineering Chemistry Fundamentals, 13,* 278–282.

Jiang, C., Alexander, R., Kagi, R. I., & Murray, A. P. (1998). Polycyclic aromatic hydrocarbons in ancient sediments and their relationships to palaeoclimate. *Organic Geochemistry, 29,* 1721–1735.

Jiménez, A., Martínez-Tarazona, R., & Suárez-Ruiz, I. (1999). Paleoenvironmental conditions of Puertollano coals (Spain): Petrological and geochemical study. *International Journal of Coal Geology, 41,* 189–211.

Kalkreuth, W. D. (1982). Rank and petrographic composition of selected Jurassic-Lower Cretaceous coals of British Columbia, Canada. *Bulletin Canadian Petroleum Geology, 30,* 112–139.

Karayigit, A. I., Spears, D. A., & Booth, C. A. (2000). Distribution of environmental sensitive trace elements in the Eocene Sorgun coals, Turkey. *International Journal of Coal Geology, 42,* 297–314.

Kemezys, M., & Taylor, G. H. (1964). Occurrence and distribution of minerals in some Australian coals. *Fuel, 38,* 389–397.

Ketris, M. P., & Yudovich, Y. E. (2009). Estimations of Clarkes for Carbonaceous biolithes: World average for trace element contents in black shales and coals. *International Journal of Coal Geology, 78,* 135–148.

Kolker, A., Palmer, C. A., & Ruppert, L. F. (2003). Modes of Occurrence of Trace Elements in Coals. In *USGS short course C*. Denver: US Geological Survey.

Li, X., Dai, S., Zhanga, W., Li, T., Zheng, X., & Chen, W. (2014). Determination of As and Se in coal and coal combustion products using closed vessel microwave digestion and collision/reaction cell technology (CCT) of inductively coupled plasma mass spectrometry (ICP-MS). *International Journal of Coal Geology, 124,* 1–4.

Liu, J., Yang, Z., Yan, X., Ji, D., Yang, Y., & Hu, L. (2015). Modes of occurrence of highly-elevated trace elements in superhigh-organic-sulfur coals. *Fuel, 156,* 190–197.

Lorenzo, E. (2012). *Geoquímica y petrografía orgánicas de los carbones de los mantos 9, 14 y 15 de la mina "La Ballesta" (Cuenca Peñarroya): Implicaciones paleoambientales y paleodeposicionales*. Unpublished M.Sc. thesis. Huelva: Universidad de Huelva.

Lyons, P. C., Palmer, C. A., Bostick, N. H., Fletcher, J. D., Dulong, F. T., Brown, F. W., et al. (1989). Chemistry and origin of minor and trace elements in vitrinite concentrates from a rank series from the Eastern United States, England and Australia. *International Journal of Coal Geology, 13,* 481–527.

Marques, M.M. (1993). *Contribuçao para o conhecimiento da petrología dos carvoes da Bacia de Peñarroya–Belmez–Espiel (Cordova-Espanha)*. Unpublished Doctoral thesis. Oporto: Universidade do Porto.

Marques, M. M. (2002). Coal facies and depositional environments of the Aurora and Cabeza de Vaca Units, Peñarroya–Belmez–Espiel Coalfield (Córdoba, Spain). *International Journal of Coal Geology, 48,* 197–216.

Martínez-Poyatos, D.J (2002). *Estructura del borde meridional de la Zona Centroibérica y su relación con el contacto entre las zonas Centroibérica y de Ossa Morena. Serie Nova Terra n° 18*. Coruña: Edicios do Castro.

Meyers, P. A., & Ishiwatari, R. (1993). Lacustrine organic geochemistry—an overview of indicators of organic matter sources and diagenesis in lake sediments. *Organic Geochemistry, 20,* 867–900.

Moore, T. A., & Shearer, J. C. (2003). Peat/coal type and depositional environment—are they related? *International Journal of Coal Geology, 56,* 233–252.

Noble, R.A. (1986). *A geochemical study of bicyclic alkanes and diterpenoid hydrocarbons in crude oils, sediments and coals*. Unpublished Doctoral thesis. Preth: The University of Western Australia.

Noble, R. A., Alexander, R., & Kagi, R. I. (1987). Configurational isomerization in sedimentary bicyclic alkanes. *Organic Geochemistry, 11,* 151–156.

O'Keefe, J. M. K., Bechtel, A., Christanis, K., Dai, S., DiMichele, W. A., Eble, C. F., et al. (2013). On the fundamental difference between coal rank and coal type. *International Journal of Coal Geology, 118,* 58–87.

Ortuño, M.G. (1971). Middle Westphalian strata in south-west Spain. In *Compte Rendu 6° Congrès International de Stratigraphie et Gèologie du Carbonifère, Sheffield 1967, III* (pp. 1275–1292).

Ourisson, G., & Albrecht, P. (1992). Hopanoids. 1. Geohopanoids: The most abundant natural products on earth? *Accounts of Chemical Research, 25,* 398–402.

Peters, K., Walters, C., & Moldowan, J. (2005). *The biomarker guide: Biomarkers and isotopes in petroleum systems and earth history*. Cambridge: Cambridge University Press.

Petersen, H. I., & Rosenberg, P. (1998). Reflectance retardation (suppression) and source rock properties related to hydrogen-enriched vitrinite in Middle Jurassic coals, Danish North Sea. *Journal of Petroleum Geology, 21,* 247–263.

Piovano, E., Ross, R., Guevara, R., Arribére, M., & Depetris, P. (1999). Geochemical tracers of source rocks in a Cretaceous to Quaternary sedimentary sequence (Eastern Sierras Pampeanas, Argentina). *Journal of South American Earth Sciences, 12,* 489–500.

Radke, M., Rullkötter, J., & Vriend, S. P. (1994). Distribution of naphthalenes in crude oils from the Java Sea: Source and maturation effects. *Geochimica et Cosmochimica Acta, 58,* 3675–3689.

Radke, M., Welte, D. H., & Willsch, H. (1982a). Geochemical study on a well in the Western Canada Basin: Relation of the aromatic distribution pattern to maturity of organic matter. *Geochimica et Cosmochimica Acta, 46,* 1–10.

Radke, M., Willsch, H., & Leythaeuser, D. (1982b). Aromatic components of coal: relation of distribution pattern to rank. *Geochimica et Cosmochimica Acta, 46,* 1831–1848.

Rimmer, S. M., & Davis, A. (1988). The influence of depositional environments on coal petrographic composition of the Lower Kittanning seam, western Pennsylvania. *Organic Geochemistry, 12,* 375–387.

Romero-Sarmiento, M. F., Riboulleau, A., Vecoli, M., Laggoun-Défarge, F., & Versteegh, G. J. M. (2011). Aliphatic and aromatic biomarkers from Carboniferous coal deposits at Dunbar (East Lothian, Scotland): Palaeobotanical and palaeoenvironmental significance. *Palaeogeography, Palaeoclimatology, Palaeoecology, 309,* 309–326.

Shao, L., Jones, T., Gayer, R., Dai, S., Li, S., Jiang, Y., et al. (2003). Petrology and geochemistry of the high-sulfur coals from the Upper Permian carbonate coal measures in the Heshan Coalfield, southern China. *International Journal of Coal Geology, 55,* 1–26.

Spears, D. A., & Zheng, Y. (1999). Geochemisty and origin of elements in some UK coals. *International Journal of Coal Geology, 38,* 161–179.

Stach, E., Mackowsky, M Th, Teichmüller, M., Taylor, G. H., Chandra, D., & Teichmüller, R. (1982). *Textbook of coal petrology* (3rd ed.). Berlin: Gebruder Borntraeger.

Stampfli, G. M., & Borel, G. D. (2002). A plate tectonic model for the Paleozoic and Mesozoic constrained by dynamic plate boundaries and restored synthetic oceanic isochrones. *Earth and Planetary Science Letters, 196,* 17–33.

Stanton, R. W., & Finkelman, R. B. (1995). Coal quality. In A. Bisio & S. Boots (Eds.), *The encyclopaedia of energy and the environment* (pp. 684–691). New York: Wiley.

Suárez-Ruiz, I., Flores, D., Marques, M. M., Martínez-Tarazona, M. R., Pis, J., & Rubiera, F. (2006). Geochemistry, mineralogy and technological properties of coals from Rio Maior (Portugal) and Peñarroya (Spain) basins. *International Journal of Coal Geology, 67,* 171–190.

Suárez-Ruiz, I., Iglesias, M. J., Jiménez, A., Laggoun-Defarge, F., & Prado, J. G. (1994). Influence of resinite on huminite properties. *Energy and Fuels, 8,* 1417–1424.

Suárez-Ruiz, I., & Jiménez, A. (2004). Coal facies studies in Spain. *International Journal of Coal Geology, 58,* 31–39.

Swaine, D. J. (1990). *Trace elements in coal*. London: Butterworth & Co., Publishing.

Taylor, G. H., Liu, S. Y., & Diessel, C. F. K. (1989). The cold-climate origin of inertinite-rich Gondwana coals. *International Journal of Coal Geology, 11,* 1–22.

Teichmüller, M. (1987). Recent advances in coalification studies in their applications to geology. In A. C. Scott (Ed.), *Coal and coal-bearing strata: Recent advances* (pp. 127–170). Oxford: Geological Society Special Publication 32, Blackwell Scientific Publications.

Tissot, B. P., & Welte, D. H. (1984). *Petroleum formation and occurrence* (2nd ed.). New York: Springer.

van Aarssen, B. G. K., & de Leeuw, J. W. (1992). High-molecular mass substances in resinites as possible precursors of specific hydrocarbons in fossil fuels. *Organic Geochemistry, 19,* 315–326.

Vassilev, S. V., Yossifova, M., & Vassileva, C. (1994). Mineralogy and geochemistry of Bobov Dol coals, Bulgaria. *International Journal of Coal Geology, 26,* 185–214.

Vliex, M., Hagemann, H. W., & Püttmann, W. (1994). Aromatized arborane/fernane hydrocarbons as molecular indicator of floral changes in Upper Carboniferous/Lower Permian strata of the Saar-Nahe Basin, South West Germany. *Geochimica et Cosmochimica Acta, 58,* 4689–4702.

Wagner, R. H. (1999). Peñarroya, a strike-slip controlled basin of early Westphalian age in Southwest Spain. *Bulletin of the Czech Geological Survey, 74,* 87–108.

Wagner, R. H. (2004). The Iberian Massif: a Carboniferous assembly. *Journal of Iberian Geology, 30,* 93–108.

Wagner, R. H. (2013). El significado geológico de las cuencas carboníferas con flora fósil en Sierra Morena. XXIX Jornadas de Paleontología. Simposio del proyecto PICG 596. *Libro de resúmenes*, 40–55.

Wagner, R. H., & Álvarez-Vázquez, C. (2010). The Carboniferous floras of the Iberian Peninsula: A synthesis with geological connotations. *Review of Palaeobotany and Palynology, 162,* 239–324.

Ward, C. R. (1989). Minerals in bituminous coals of the Sydney basin (Australia) and the Illinois basin (USA). *International Journal of Coal Geology, 13,* 455–479.

Ward, C. R., Bocking, B., & Ruan, C. (2001). Mineralogical analysis of coals as an aid to seam correlation in the Gloucester Basin, New South Wales, Australia. *International Journal of Coal Geology, 47,* 31–49.

Ward, C. R., & Christie, P. J. (1994). Clays and other minerals in coal seams of the Moura-Baralaba area, Bowen Basin, Australia. *International Journal of Coal Geology, 25,* 287–309.

Ward, C. R., Corcoran, J. F., Saxby, J. D., & Read, H. W. (1996). Occurrence of phosphorus minerals in Australian coal seams. *International Journal of Coal Geology, 31,* 185–210.

Ward, C. R., Spears, D. A., Booth, C. A., Staton, J., & Gurba, L. W. (1999). Mineral matter and trace elements in coals of the Gunnedah Basin, New South Wales, Australia. *International Journal of Coal Geology, 40,* 281–308.

Wedepohl, K. H. (1978). *Handbook of geochemistry* (Vol. II). Berlin: Springer.

Winston, R. B. (1986). Characteristic features and compaction of plant tissues traced from permineralized peat to coal in

Pennsylvanian coals (Desmoinesian) from the Illinois Basin. *International Journal of Coal Geology, 6,* 21–41.

Winston, R. B. (1988). Paleoecology of Middle Pennsylvanian-age peat-swamp plants in Herrin coal, Kentucky, USA. *International Journal of Coal Geology, 10,* 203–238.

Yudovich, Y. E., & Ketris, M. P. (2006). Chlorine in coal: A review. *International Journal of Coal Geology, 67,* 127–144.